2023-01-0205 Published 11 Apr 2023

Multi-Dimensional Spark Ignition Model for Arc Propagation and Thermal Energy Deposition with Crossflow

Kyeongmin Kim, Corey Tambasco, Matthew Hall, and Ron Matthews Univ. of Texas-Austin

Citation: Kim, K., Tambasco, C., Hall, M., and Matthews, R., "Multi-Dimensional Spark Ignition Model for Arc Propagation and Thermal Energy Deposition with Crossflow," SAE Technical Paper 2023-01-0205, 2023, doi:10.4271/2023-01-0205.

Received: 07 Nov 2022 Revised: 13 Jan 2023 Accepted: 01 Feb 2023

Abstract

A multi-dimensional model of the spark ignition process for SI engines was developed as a user defined function (UDF) integrated into the commercial engine simulation software CONVERGE CFD. The model simulates spark plasma movement in an inert flow environment without combustion. The UT model results were compared with experiments for arc movement in a crossflow and also compared with calorimeter measurements of thermal energy deposition under quiescent conditions. The arc motion simulation is based on a mean-free-path physical model to predict the arc movement given the contours of the crossflow velocity through the gap and the interaction of the spatially resolved electric field with the electrons making up the arc. A further development is the inclusion of a model for the thermal energy deposition of the arc as it is stretched by the interaction of the flow and the electric field. A novel feature of this model is that the thermal energy delivered to the gap at the start of the simulation is distributed uniformly along the arc rather than at discrete points along the arc, as is the case with the default CONVERGE CFD ignition models. This feature was found to greatly reduce the tendency of the arc to distort its shape and tangle itself in a non-physical way, as is the tendency when discrete energy input is used. It was found that the tangled distortion of the arc when using discrete energy input was due to perturbations along the arc caused by differential expansion of the gas along groups of adjacent mesh cells that either had energy input or did not. The distributed energy feature also gave arc temperature distributions that were more spatially uniform and had steeper temperature gradients, consistent with experimental arc images. The results are compared with experimental high-speed video images of arc movement for a spark plug of similar geometry and taken over a range of pressures and crossflow velocities in a high-pressure constant volume vessel. There is good agreement between the simulations and experimental images for the arc stretch distance in response to a crossflow. The simulations did not display as much lateral arc dispersion as seen in the experimental results, however, that were perhaps associated with flow recirculation zones downstream of the gap, present in the experiments. The influence of the electric field was shown by turning off the electric field effect in the simulations such that the arc movement was influenced by the flow field alone. The effect of the electric field was found to be more pronounced at lower crossflow velocities of 5 m/s and at lower pressures.

Introduction

There is increasing interest in the details of the spark ignition process in spark ignition engines as newer engines are designed to operate under more extreme in-cylinder conditions, elevated boost pressure, and lean or dilute mixtures. These conditions make the spark ignition more challenging in terms of reliable ignition and combustion with minimum cycle-to-cycle variations. Research on the spark ignition process to understand its characteristics has been conducted by many researchers using both experiments and simulations.

Detailed ignition sub-models can be integrated with computational fluid dynamics (CFD) software such as CONVERGE™ CFD, to simulate the ignition process. Many researchers have investigated and modeled spark channel behavior within the local flow and its effects on the flame kernel development. Fan et al. introduced a Discrete Particle Ignition Kernel (DPIK) model where the flame kernel is assumed to be spherical and is described using discrete particle markers [1]. This Lagrangian particle approach made it less sensitive to numerical mesh size. Duclos et al. proposed an Arc and Kernel Tracking Ignition Model (AKTIM) for describing the flame kernel expansion [2]. The spark is modeled by a set of particles along the spark path that can be elongated by the mean flow field. Their model also includes the secondary side of the electrical inductive ignition system. Each particle receives energy from the partially simulated ignition circuit. Dahms et al. developed a Spark Channel Ignition Monitoring Model (SparkCIMM) which models the spark channel with discrete particles [3]. These particles can

also be stretched by the local flow. Restrike of the stretched spark channel is modeled in SparkCIMM by resetting the spark marker particles to their original location when the spark channel exceeds a predefined length. The spark energy deposition rate was assumed to be uniform along the spark channel and constant in time. Lucchini et al. also introduced a model for ignition and flame kernel development [4]. The spark channel was modeled with discrete particles which receive energy from a simplified ignition circuit model. Restrike of the stretched spark channel was modeled with two different criteria, column voltage and the maximum channel length. However, it does not include a model for short-circuiting. Numerical studies using an Energy Deposition Model were conducted recently to simulate the spark ignition process in an engine [5,6]. Energy is deposited into a spherical energy source with the energy deposition rate determined from the measured voltage and current. Scarcelli et al. showed that the Lagrangian-Eulerian Spark-Ignition (LESI) model is in good agreement with visualized experiments for non-quiescent, engine-like conditions [7]. However, short-circuit and restrike behavior were not included in this model. Sforza et al. [8] used Lucchini's model, briefly discussed above, to investigate the flame kernel development and flame stretch in combustible gas mixtures. Masuda et al. [9] developed a model of restrike and short-circuit behavior based on the voltage across the spark channel. They used the ignition circuit model proposed by Duclos et al. [2], which includes only the secondary side of the electrical inductive ignition system. Arai et al. used Direct Numerical Simulation (DNS) and the Lagrangian tracking method, with 11 particles spaced evenly between the electrodes at breakdown, to investigate the spark path with stretching and short circuiting for a crossflow velocity of 15 m/s [10]. They used an "equivalent circuit" model that is simplified relative to the more comprehensive ignition circuit model developed by our research team [11]. They observed repetition of elongation and short circuiting of the discharge path. However, their study was conducted for a single pressure. They also studied the influence of electrode shape and permeability on discharge characteristics.

There have been several studies related to the flow around the spark plug gap and the effect of the local flow on the spark kernel movement and flame kernel formation. Mantel found that the orientation of the spark plug relative to the mean flow changes the mean flow field around the spark plug gap and the heat transfer to the electrode [12]. These are important factors in the development of the initial flame. Kim and Anderson investigated the method to determine the gas velocity near the spark plug gap using voltage and current profiles, known as spark anemometry [13]. The velocity predicted by their spark plug anemometry was always lower than the velocity measured by Hot Wire Anemometry (HWA). Gardiner et al. showed improvements of spark anemometry using a constant current spark and high-speed video [14]. From the high-speed video, they found that the velocity of the spark head (the leading edge of the spark channel during crossflow) is about one-half of the freestream velocity.

Many researchers investigated the behavior of restrike and short-circuit of the stretched arc using both experiments and simulations. Shiraishi et al. studied the effects of gas pressure, gas flow velocity, and discharge current on spark channel formation, focusing on spark channel stretch and restrike events using a constant volume chamber and a single cylinder engine [15]. They found that the stretching of the spark channel defined by channel tip velocity does not follow the gas flow velocity at low pressure compared to high pressure. Restrike voltage was found to be smaller than the breakdown voltage at the same pressure. The voltage rise rate at the same velocity was higher for high pressure compared to low pressure, which means the spark channel stretches faster at high pressure. However, pressure and velocity were limited to 1000 kPa and 7.9 m/s. Sandhu et al. investigated the flow field around the spark plug and its effect on spark behavior using Particle Image Velocimetry (PIV) in steady flow bench tests and in an engine motoring condition [16]. Spark stretch length and restrike frequency increased with increasing mean flow velocity. They also found that the first restrike event occurred faster after breakdown at a higher current level with increasing mean flow velocity. These findings are consistent with results from Shiraishi et al. [15]. They went up to 50 m/s of crossflow velocity; however, the pressure was limited to ambient pressure. Huang et al studied short-circuit and restrike phenomena with different flow velocities, gap sizes, and discharge energies [17]. The short-circuit and restrike decreased with increase of discharge power and increase of spark gap size. Restrike voltage increased with decreasing discharge current and increasing flow velocity. Spark channel growth rate was proportional to the gas flow velocity. They also proposed a new spark plug prototype with a triangular electrode head, which is beneficial for suppressing the short-circuit. Wörner and Rottenkolber used a spark plug as an anemometry to measure turbulent flow in internal combustion engines [18]. They developed a correlation between spark voltage and flow velocity at various pressures and currents using image and signal processing. They found that increasing pressure results in a more rapid voltage rise, which means more elongation of the spark channel. On the other hand, increasing current resulted in slower voltage rise and arc stretch. They used this setup and the derived correlation between voltage and velocity to measure the turbulence intensity in an internal combustion engine with different charge motion setups. Sayama et al. developed models for short-circuiting and blow-out of spark channels [19]. Their short-circuit model was based on the number and the spread of the electrically charged particles distributed within the plasma arc. Their blow-out model was based on Townsend discharge theory and diffusion of electrons and positive ions in the spark channel. The optically measured length of the spark channel was used to validate the models against experimental results. They also suggested a modified equation for spark channel resistance, originally developed by Kim et al. [13], for better prediction at high-velocity flow conditions. Zembi et al. investigated pressure and flow field effects on arc channel characteristics for a J-type spark plug using both experiments and simulations for pressures up to 8 bar and for a velocity of 13.2 m/s [20]. The Imposed Stretch Spark Ignition Model (ISSIM) method developed by Colin and Trufin [21] was used for simulating arc stretch using CONVERGE CFD. They found that the discharge duration decreases as the pressure increases. The ISSIM for arc simulation showed good agreement with experiments in terms of arc length and the model predicted

the restrike event at 1 bar and 13.2 m/s fluid flow condition. They investigated the effect of pressure with 1, 4, and 8 bar. However, they only used one velocity condition at 13.2 m/s and the effect of flow velocity is still unknown.

Arc propagation and its energy deposition can be simulated using a thermal plasma modeling solver, VizSpark, which solves electromagnetic equations along with a laminar flow field. However, it takes about a week for a few milliseconds of simulation even with a high-performance supercomputer [22]. The arc propagation model in the present study was developed to simulate similar arc propagation as VizSpark in much less time with the multidimensional simulation software CONVERGE CFD.

The present study investigated arc propagation for various pressures and crossflow velocities experimentally. Images from a high-speed camera revealed that the arc propagation depends on both pressure and crossflow velocity. A new arc propagation model was developed based on the mean free path of gas molecules and collisions between electrons and gas molecules. The results from simulations using this new arc propagation model were compared with experimental results. The new arc propagation model was able to investigate the effect of the electric field on arc propagation, which acts against the arc propagation by the crossflow.

The presented arc propagation model is integrated into the CFD software, CONVERGE CFD to simulate the arc propagation under the presence of crossflow. A similar simulation could be done using the thermal plasma solver, VisSpark (Esgee Technologies). However, the VizSpark simulation requires much more time and computing resources than the simulation using CONVERGE CFD with the presented model.

Because the model is already integrated into CONVERGE CFD as a user-defined-function (UDF), its implementation within a full engine simulation that includes flow and combustion processes is straight forward and will be the subject of future work.

The simulation using the presented geometry took about 4 hours on a 128 core supercomputer. Similar simulations using a thermal plasma modeling solver (VizSpark) required 4 days on a less powerful computer. A rough estimate for the simulation time for the thermal plasma model using the same 128 core supercomputer is about 30 hours.

Experimental Measurement

The experimental setup is shown in Figure 1. The constant volume combustion vessel has a cylindrical shape with diameter of 7.9 cm and height of 1.4 cm. The spark plug was located at the center of one of the disk-shaped sidewalls. Quartz windows allowed optical access to the spark plug. The nitrogen flow from the high-pressure cylinder was introduced to the spark plug gap in the combustion vessel by a copper tube. The spark plug and tube were aligned to have the nitrogen directed to the center of the spark plug gap. The J-gap ground electrode was placed perpendicular to the incoming crossflow to minimize flow disturbance by the electrodes. The pressure

FIGURE 1 Experimental setup

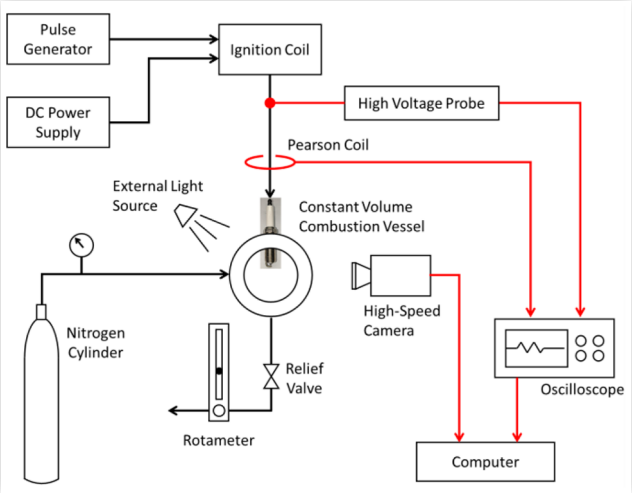

regulator and a relief valve at the outlet of the vessel controlled the pressure inside the vessel and the gas flow rate. The flow rate was measured with a rotameter located downstream from the relief valve. The rotameter was calibrated with a diaphragm-type gas meter. The free flow velocity out of the gas supply tube was calculated based on the measured flow rate and the diameter of the tube. The rotameter was calibrated for pressures up to 30 bar and for velocities up to 30 m/s.

Visualization of spark column stretch under crossflow was done using a Photron Fastcam Mini high-speed camera. The optical path of the camera was set to capture the side view of the spark plug gap. The frame rate of the camera was set to 50,000 frames per second (FPS) to capture the milliseconds-order spark event. An external light source was used to capture the outline of the spark plug and electrodes.

A Tektronix Model P6015A high voltage probe measured the breakdown and follow-on voltages at the top of the spark plug. A Pearson Model 110 current sensor was used to measure the discharge current. The voltage and current signals were recorded using a 100 MHz 4-channel Tektronix oscilloscope. Breakdown voltages were recorded separately since a faster time-base setting was needed to resolve these very short duration events.

All of the measurements were made using a Bosch OEM 14 mm spark plug designed for natural gas engines. The spark plug had a J-type ground electrode with 2 mm width and the stepped center electrode had 0.6 mm and 2 mm diameters. The dwell time used was 4 ms. Nitrogen was used for all of the measurements of spark column behavior without combustion. The experiments were conducted for pressures of 6, 12, and 20 bar and crossflow velocities of 5, 10, and 15 m/s.

Video captured by the high-speed camera was processed frame-by-frame to eliminate the electrodes from the image. Then we could obtain an image of only the plasma arc in the frame. The area occupied by the spark column and perimeter of the spark column in the frame was measured to get the length and thickness of the equivalent rectangular spark column that has the same area and perimeter as those measured.

The first data we could extract from the experiments were the discharge duration and number of short-circuits during

TABLE 1 Number of short-circuits and discharge duration

	5 m/s	10 m/s	15 m/s
6 bar	1 / 2.54 ms	8 / 2.14 ms	9 / 1.56 ms
12 bar	3 / 1.66 ms	3 / 1.16 ms	6 / 1.20 ms
20 bar	2 / 1.54 ms	2 / 1.10 ms	4 / 0.94 ms

the discharge, as shown in Table 1. The discharge duration shortens with increasing crossflow velocity. The spark column stretches further and faster with higher crossflow velocity. Higher voltage of the stretched arc consumes electrical energy stored in the ignition coil faster, resulting in shorter discharge duration. The discharge duration also changes with gas pressure. The gap voltage for a given arc length increases with increasing pressure. The discharge duration decreases with higher gap voltage in the same manner explained above. The number of restrikes/short-circuits tends to increase with increasing crossflow velocity. The spark column stretches faster with higher crossflow velocity resulting in more frequent restrikes/short-circuits. These observations are consistent with other researchers [15,16]. However, the relationship between the number of restrikes/short-circuits and pressure shows different behavior between low and mid/high velocity. For 10 and 15 m/s, the number of restrikes/short-circuits decreases with increasing pressure. This is because the arc needs to be stretched further for a restrike or short-circuit at higher pressure. Figure 2 shows images at the time of first short-circuit after breakdown. For a given pressure and velocity, two images with 0.02 ms interval are shown to illustrate the arc path difference between before and after the short-circuit. The spark column stretched further before the first short-circuit occurs, especially at 20 bar.

One special case we observed from the experiments was with 6 bar pressure and 5 m/s crossflow velocity. Images from the experiment with 0.4 ms increments are shown in Figure 3.

FIGURE 2 First short-circuit event at various pressures and crossflow velocities. Two images are shown at each combination of pressure and crossflow velocity, 0.02 ms apart, with one before and the other after.

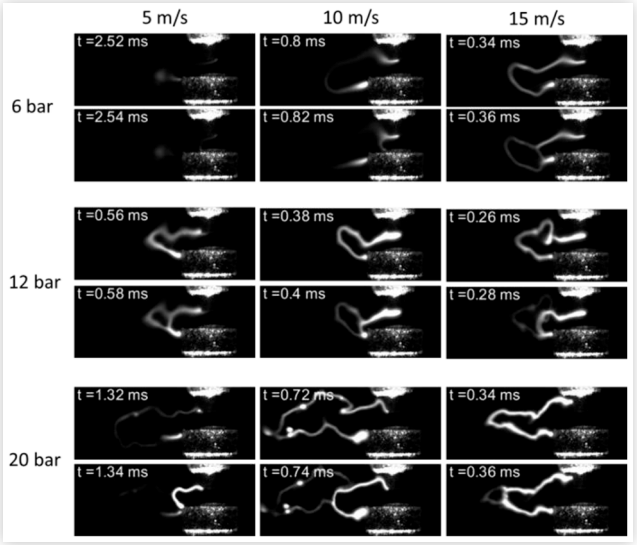

FIGURE 3 Arc stretch at 6 bar pressure and 5 m/s crossflow velocity

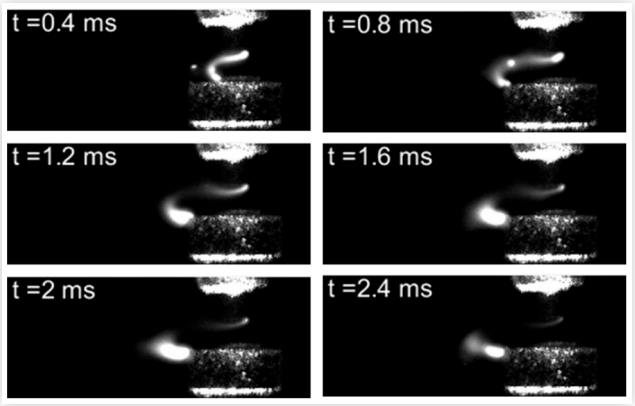

FIGURE 4 Arc stretch at 0.26 ms after breakdown for various pressures and crossflow velocities

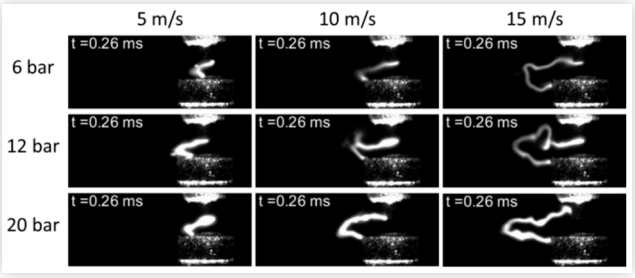

The discharge duration for this case was 2.54 ms. The arc length or stretch distance does not change much compared to other pressures and velocities. The spark column rather maintains its position after 1.2 ms until the end of discharge.

Figure 4 shows images at 0.26 ms after breakdown for various pressures and crossflow velocities to show differences in stretch distance. Restrike/short-circuit does not occur until after 0.26 ms for all the conditions. Therefore Figure 4 shows pure arc stretch without a restrike or short-circuit for all the conditions. These 9 images reveal that arc stretch depends on both pressure and velocity. The arc stretches farther with higher pressure and higher crossflow velocity. These findings and the special arc behavior at 6 bar and 5 m/s led us to develop a new arc propagation model.

Arc Propagation Model

The basic idea of this new arc propagation model, based on the mean-free-path of gas molecules and collisions between electrons and gas molecules, is shown in Figure 5. The velocity of the gas molecules is much smaller than the velocity of the electrons. Therefore, the gas molecules can be assumed as stationary compared to electrons. Electrons traveling from the cathode to the anode collide with gas molecules between the gap. The travelling distance of an electron between two consecutive collisions can be assumed as the mean free path

FIGURE 5 Schematic of the arc propagation model based on the mean-free-path of a gas molecule and collisions between electrons and gas molecules

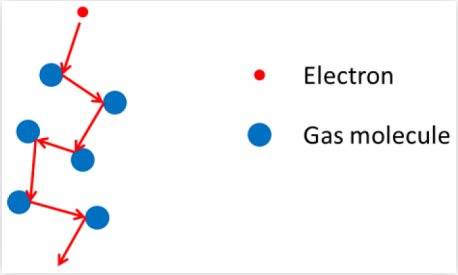

of the gas molecules. If we imagine a spark plug placed vertically in space, electrons will travel in the z direction. Then in a quiescent condition with no crossflow, the electron's travel distance in the x and y directions is zero, as the sum of the deflected direction and distance of each electron is zero in the x and y directions.

Next, we can introduce a crossflow condition between the gap. If the crossflow velocity only has an x component, electrons will be deflected only in the x direction compared to the quiescent no crossflow condition. This deflection of electrons or stretch of the arc is proportional to the mean free path of the gas molecules, λ, and the total number of collisions, N. The total number of collisions can be expressed in terms of the time-step in the simulation, Δt, and collision frequency between gas molecules and electrons, $\dot{N}$.

$$\Delta x \sim \lambda N = \lambda \dot{N} \Delta t \tag{1}$$

Additionally, we can introduce another term that is related to the crossflow velocity, v_f, but made dimensionless using the molecular velocity, v_m. A gas molecule in a quiescent condition can be considered to have molecular velocity in the +x and -x directions with one-half probability in each direction. Then the combined velocity of molecular velocity and crossflow velocity are $v_m + v_f$ and $v_m - v_f$ in the +x and -x directions, respectively. Then we can get the probability of deflected direction in the +x direction as

$$P_f = \frac{v_m + v_f}{(v_m + v_f) + (v_m - v_f)} = \frac{v_m + v_f}{2v_m} \tag{2}$$

Combining these two equations (1) and (2) results in the following equation (3).

$$\Delta x \sim \lambda \dot{N} \Delta t \left(P_f - 0.5\right) \tag{3}$$

One-half is subtracted from P_f to have $\Delta x = 0$ when $v_f = 0$ in the quiescent no crossflow condition.

This expression of deflected distance of an electron after collision with a gas molecule is based on one electron and one gas molecule with a crossflow velocity v_f and molecular velocity v_m as shown in Figure 6(a) with Δx in equation (3). However, the actual plasma arc consists of multiple electrons emitted continuously from the cathode. The deflected distance of a group of multiple electrons colliding with a single gas

FIGURE 6 Deflected distance of an electron for (a) Single Electron Single Molecule, (b) Multiple Electrons Single Molecule, (c) Single Electron Multiple Molecules, (d) Multiple Electrons Multiple Molecules

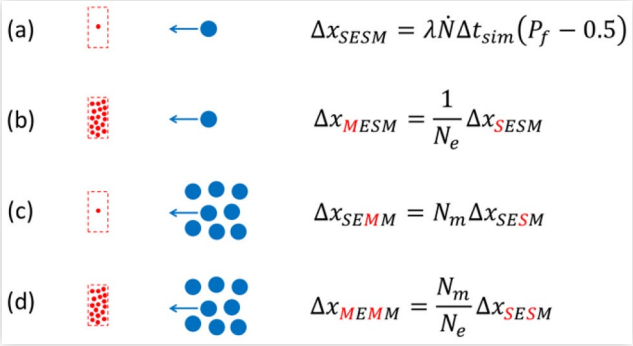

molecule can be expressed as $\Delta x/N_e$, where N_e is the number of electrons as in Figure 6(b). Similarly, the deflected distance of a single electron colliding with a group of multiple gas molecules can be expressed as $\Delta x \times N_m$, where N_m is the number of gas molecules as in Figure 6(c). Combining these two ideas, the deflected distance of a group of multiple electrons colliding with a group of multiple gas molecules can be expressed as $\Delta x \times N_m/N_e$ as in Figure 6(d). We can replace N_m/N_e with n_m/n_e where n_m is the number density of gas molecules and n_e is the number density of electrons in the plasma arc. n_m can be calculated given the pressure and temperature. n_e can be calculated given the current, arc diameter, and electron velocity. Current is solved simultaneously with the flow field using our ignition circuit model developed previously [11]. The arc diameter in this model is assumed to be constant at 100 µm. The electron velocity and collision frequency used in equation (3) are derived using an analogy from molecular gas dynamics as shown in Figure 7.

Electrons are much smaller and much faster than gas molecules. Thus, the electron diameter and molecular velocity are negligible. These two ideas lead to a difference in expression for collision frequencies $\dot{N}_m$ and $\dot{N}_e$. Molecular velocity can be calculated using the Boltzmann constant, temperature, and mass of a gas molecule. Electron velocity can be expressed in terms of electron charge q, electric field strength E, mass

FIGURE 7 Comparison between inter-molecular collision and electron-molecular collision

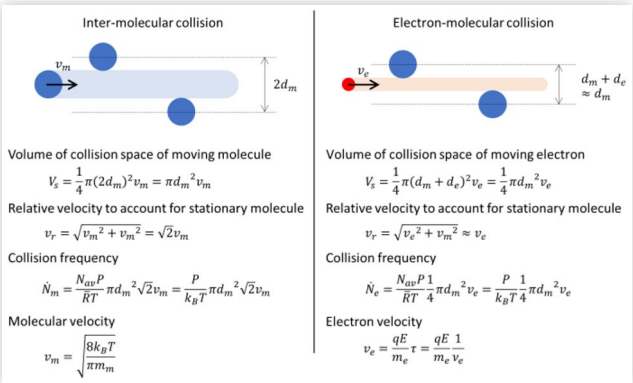

of an electron m_e, and time between two consecutive collisions τ, which is the inverse of the collision frequency $\dot{N}_e$. Using two equations for collision frequency and electron velocity, we can get equation (4) for electron velocity in terms of temperature, pressure, and electric field strength, where electric field strength can be replaced with voltage across the gap divided by arc length.

$$v_e = \sqrt{\frac{qE}{m_e}\frac{4k_BT}{P}\frac{1}{\pi {d_m}^2}} \tag{4}$$

Electron movement is not solely determined by collision with gas molecules. Electrons travel from cathode to anode along the electric field. In a quiescent condition without crossflow, electrons will travel straight from cathode to anode. However, once the arc is stretched due to crossflow, electrons in the arc lie in space where the electric field is curved from cathode to anode. The direction of the electric field at location x can be expressed as,

$$\hat{x}_E = \frac{d_a}{\sqrt{d_c^2 + d_a^2}}\hat{x}_c + \frac{d_c}{\sqrt{d_c^2 + d_a^2}}\hat{x}_a \tag{5}$$

$\hat{x}_c$ and $\hat{x}_a$ are unit vectors of direction from cathode and unit vector of direction to anode, respectively. Also, d_c and d_a are the distance from the cathode and the distance to the anode, respectively. Figure 8 shows the direction of the electric field based on equation (5). The travelling distance of an electron along the electric field can be expressed as

$$\Delta x_E \sim v_e \Delta t \tag{6}$$

Combining these two terms of electron movement due to flow and electric field, we can get equations (7), (8) and (9),

$$\Delta x_{i,arc} = \Delta x_{i,flow} + \Delta x_{i,E} \tag{7}$$

$$\Delta x_{i,flow} = C_f \frac{n_m}{n_e}\lambda \dot{N} \Delta t_{sim}\left(P_{f,i} - 0.5\right) \tag{8}$$

$$\Delta x_{i,E} = C_E v_e \Delta t_{sim} \hat{x}_{E,i} \tag{9}$$

FIGURE 8 Direction of electric field based on direction vector and distance from cathode and anode

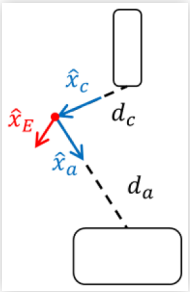

where $i = x, y, z$ direction in the coordinate system and C_f and C_E are coefficients used in the model for each term. Coefficients C_f and C_E are set to 10^{-5}. This value may seem too small. However, we interpret it as compensation for the relatively large time-step used in the simulations. Fast moving electrons will travel from cathode to anode in the order of tens of nanoseconds. If we want to track fast electrons step-by-step between the gap, we would need a time-step less than a nanosecond, which would require a lot of time for simulation. By applying these small coefficients, we can still use microsecond-order time-steps in the simulation but still estimate the arc propagation with the model. The magnitude of these coefficients, 10^{-5}, seems reasonable when we consider the number densities of molecules and electrons. We found that the number density of electrons, which depends on current, electron velocity, and arc diameter, is of the order of $10^{21}/m^3$. On the other hand, the number density of molecules, which depends on pressure and temperature, is of the order of $10^{26}/m^3$.

This model for arc propagation requires the current and voltage of the spark column solved simultaneously with the flow field. The current and voltage in the ignition circuit were calculated using our previously developed ignition circuit model [11]. The circuit model requires either arc resistance or arc voltage across the stretched arc. We can assume that the voltage of the stretched arc is proportional to arc length as the gap voltage of an unstretched arc in a quiescent condition is constant during discharge. The voltage of the stretched arc was calculated using the voltage of the unstretched arc, gap distance, and stretched arc length.

$$V_{stretched} = \frac{l_{stretched}}{d_{gap}} V_{unstretched} \tag{10}$$

The voltage of the unstretched arc was measured previously in a calorimeter with a quiescent condition [23].

A restrike or short-circuit of the plasma arc occurs when the arc is stretched far away from the gap. There are a couple of factors that affect the short-circuit voltage of the stretched arc. First is the distance between the points along the arc where a short-circuit occurs. Longer distances between the points requires a higher short-circuit voltage just like the higher breakdown voltage for larger gap sizes. Second is the charge or current flowing through the arc. Breakdown occurs when the charge stored between the two electrodes exceeds a certain value for the arc to cross the gap. The same principle can be applied to the short-circuit of the plasma arc. Charge flowing through the cross section of the arc, which is equivalent to the current, affects the short-circuit voltage. This current dependent short-circuit voltage was also studied by Sayama et al.[19]. A derivation of the short-circuit voltage starts from the capacitance equation for a parallel plate capacitor. We can assume the spark plug behaves as a parallel plate capacitor with effective area A_0. Thus, the capacitance of the spark plug can be written as equation (11).

$$C_{SP} = \frac{\varepsilon A_0}{d_{gap}} \tag{11}$$

where ε is the permittivity of the gas and d_{gap} is the gap distance of the spark plug. The capacitance can also be written as a ratio between the stored charge and the voltage.

$$C_{SP} = \frac{Q_{BD}}{V_{BD}} \tag{12}$$

The subscript BD refers to breakdown, thus Q_{BD} is the charge stored in the spark plug at breakdown and V_{BD} is the breakdown voltage. By equating equations (11) and (12), we can get the breakdown voltage equation as a function of stored charge, effective area, and gap distance.

$$V_{BD} = \frac{1}{\varepsilon}\frac{Q_{BD}}{A_0}d_{gap} \tag{13}$$

Similarly, the short-circuit voltage can also be written as a function of the stored charge per unit area and distance. A longer distance requires a higher voltage to short-circuit between those points. More charge per unit area, which is equivalent to a higher current makes it easy to short-circuit compared to a lower charge per unit area or lower current. Thus, the short-circuit voltage is proportional to the ratio between that distance and the gap distance; this ratio of the two different charge per unit area values between breakdown and short-circuit are part of equation (14).

$$V_{SC} = C_{SC}V_{BD}\frac{\frac{Q_{BD}}{A_0}}{\left(\frac{Q}{A}\right)_{SC}}\frac{d}{d_{gap}} \tag{14}$$

$\left(\frac{Q}{A}\right)_{SC}$ is the charge per unit area at short-circuit, d is the distance between short-circuit points, C_{SC} is the coefficient used in the short-circuit voltage equation. The charge per unit area of the plasma arc needs to be expressed in terms of properties of the arc. We can use the number density of electrons in the arc, n_e, arc diameter, d_{arc}, and electron charge, q as in the following equation (15).

$$\left(\frac{Q}{A}\right)_{SC} = qn_e d_{arc} \tag{15}$$

The product of three parameters, number density of electrons in 1/m^3, arc diameter in m, and electron charge in C gives charge per unit area in C/m^2. Charge per unit area of the plasma arc may not be equal to the product of those three parameters. However, any coefficient required can be integrated into C_{SC} in equation (14). We also need to evaluate the term $\frac{Q_{BD}}{A_0}$ of the spark plug at breakdown. However, we cannot get the value of Q_{BD} and A_0 individually. Instead, we can use equation (13) to get the equation for $\frac{Q_{BD}}{A_0}$.

$$\frac{Q_{BD}}{A_0} = \frac{\varepsilon V_{BD}}{d_{gap}} \tag{16}$$

Substituting equations (15) and (16) into equation (14), we get the short-circuit voltage equation with terms we can get explicitly from the simulation and experiment.

$$V_{SC} = C_{SC}V_{BD}\frac{\frac{\varepsilon V_{BD}}{d_{gap}}}{qn_e d_{arc}}\frac{d}{d_{gap}} \tag{17}$$

We found that a coefficient $C_{SC} = 5$ shows good agreement with experiments. The short-circuit voltage between the points A and B separated by distance, d is compared with the voltage along the arc between the points A and B, V_{AB}. This V_{AB} is proportional to the gap voltage, V_{gap} and the ratio between the arc length between A and B, l_{AB} and the total arc length, l_{total}. A short-circuit occurs if the V_{AB} is higher than V_{SC}.

$$V_{SC} < V_{AB} = V_{gap}\frac{l_{AB}}{l_{total}} \tag{18}$$

We were able get quite reasonable results with the model described above. However, due to the discretized nature of the simulation, the shape of the arc was still jagged and not smooth. To resolve this issue, we smoothed the arc shape by averaging spatially for the arc location. The new arc location was determined using the following equation, which means it is smoothed by a total 1% of adjacent arc locations. n is an index number of discrete points representing the spark column in the simulations.

$$\vec{x}_{n,new} = 0.005\vec{x}_{n-1} + 0.99\vec{x}_n + 0.005\vec{x}_{n+1} \tag{19}$$

The minimum and maximum distance between the points representing the arc were 20 and 40 μm, respectively, to have more points for the stretched arc. This arc propagation model was integrated into CONVERGE CFD using a user-defined function (UDF).

The arc was tracked using a discrete number of points that represent the location of the arc. The number of points change with the total length of the arc based on the minimum and maximum distance between the points. The diameter of the arc is an input from the user, which was set to 100 μm by default. The volume occupied by the plasma arc was determined by the location of the points and the specified arc diameter. Energy from the arc discharge is deposited into the cells within the volume.

Simulation Results

Simulations were conducted using the described arc propagation model for pressures of 6, 12, and 20 bar and crossflow velocities of 5, 10, and 15 m/s to compare with our experimental results. The crossflow velocity was calculated based on the measured flow rate and the diameter of the tube, and used in the simulation as a boundary condition for the flow out of the gas supply tube. However, the actual crossflow velocity between the gap was higher than the free stream velocity as the electrodes blocked and directed part of the flow [11]. A

FIGURE 9 Simulation geometry showing spark plug and tube outlet

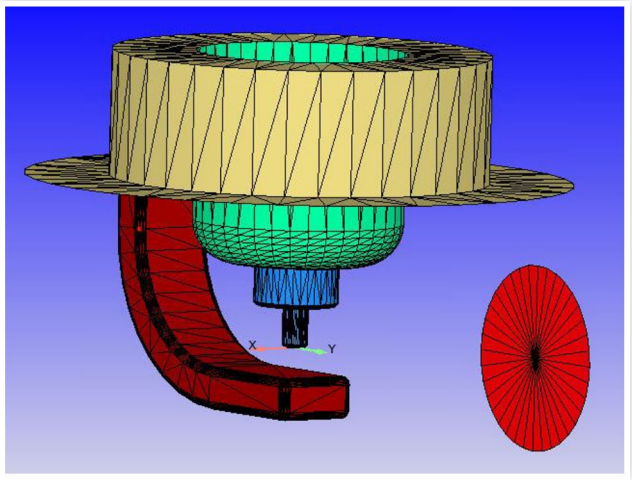

simulation domain around the spark plug was used for fast calculation. The spark plug and outlet of the tube were placed the same as in the experimental setup as shown in Figure 9. The velocity boundary for each given crossflow velocity was set at the outlet of the tube. The base mesh size in the simulation domain was 0.4 mm. A finer mesh size of 50 μm between and around the spark plug gap was used. The location of the initial breakdown was placed between the center of the cathode and the center of the anode. Our previously developed ignition circuit model and distributed energy deposition model were used together with the new arc propagation model for better estimates of current and voltage [11].

Figure 10 shows a comparison between experiment and simulation for 12 bar pressure and 10 m/s velocity. The spark column from the simulation is shown as a red line placed on top of the image from the experiment. The detailed shape of the stretched arc is slightly different from the experiment. This difference could be a result of flow field differences in the simulation and experiment around the spark plug. The spark plug was placed perpendicular to the crossflow out of the tube in the simulations. However, the actual spark plug might have been placed with a slight angle relative to the crossflow. This issue can be resolved if we introduce three x, y, and z components to the crossflow velocity. In this simulation, only the x component of crossflow velocity was used. Another possibility for the discrepancy between the simulation and experiment is the location of initial breakdown. The actual location of initial breakdown between the gap changes for each spark and cannot be predicted. It depends on various parameters such as surface roughness, electrode shape, gas molecule distribution between the gap, etc.

FIGURE 10 Arc propagation comparison between experiment and simulation (red) at 12 bar pressure and 10 m/s crossflow velocity

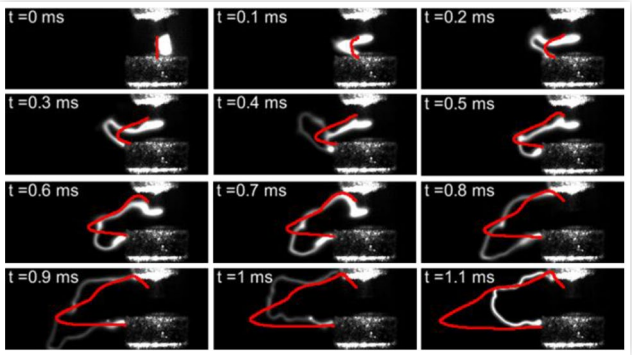

An actual spark column created at either the upstream or downstream side of the electrode will show different arc stretch behavior. That is the same for the simulation spark column created on the left and right edges of the electrode relative to the incoming crossflow.

Figure 11 shows arc length and stretch distance changes with time for both the experiment and simulation at 12 bar and 10 m/s. The first thing to note from this figure is the difference in discharge duration. The discharge duration from the simulation is longer than that from the experiment by about 0.5 ms. The discharge duration is mostly determined by how much energy and how fast it is drawn from the ignition coil

FIGURE 11 Experiment and simulation comparison for 12 bar pressure and 10 m/s crossflow velocity, (a) arc length and (b) stretch distance

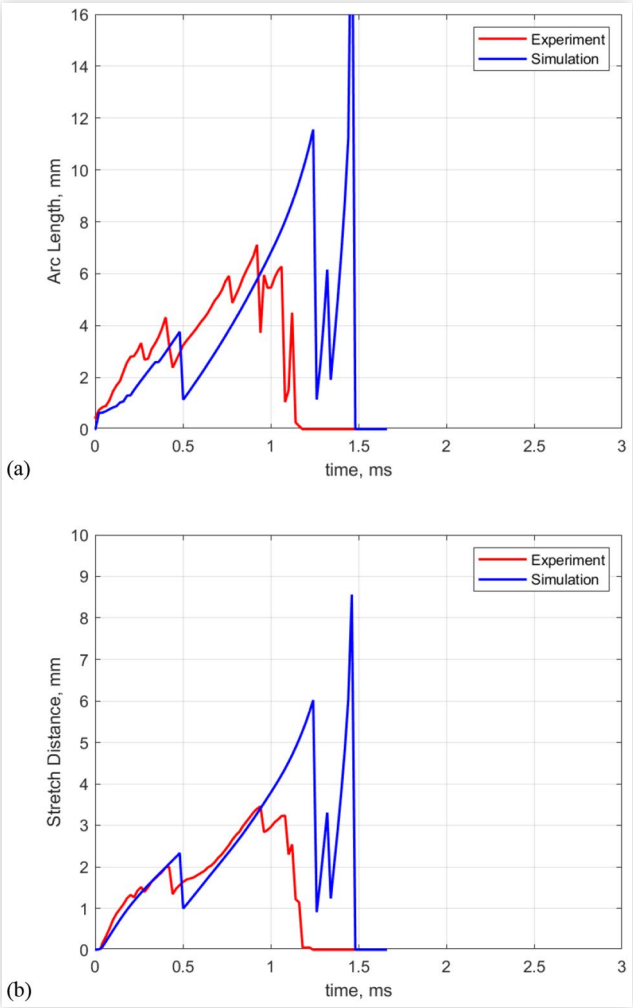

FIGURE 12 Experiment (red) and simulation (blue) comparison for various pressures and crossflow velocities (a) arc length and (b) stretch distance

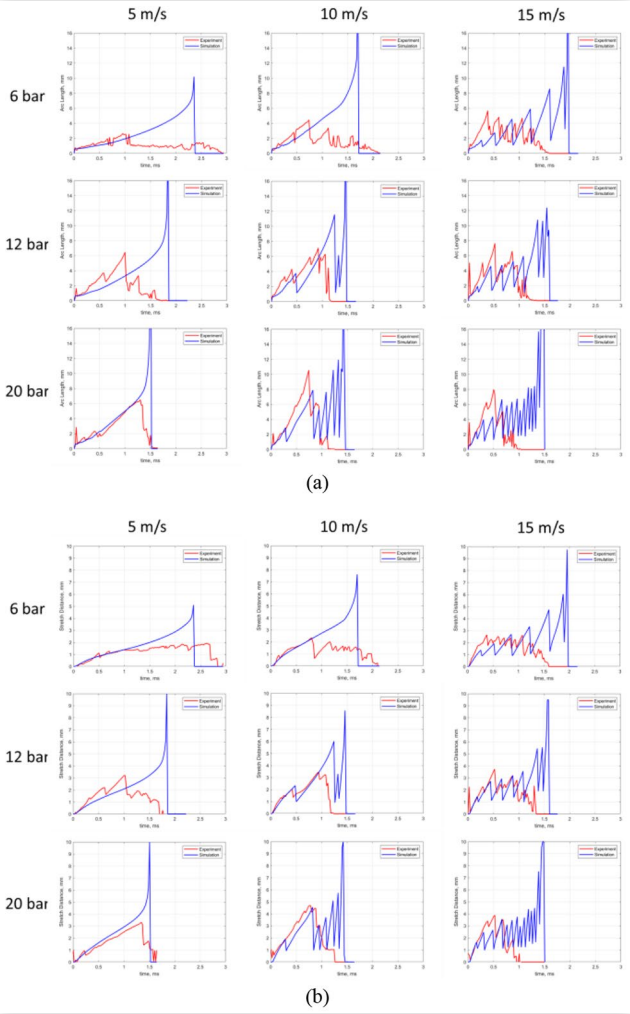

to the gas within the gap. Those depend on the voltage and current in the spark column. The voltage of the stretched arc was probably underestimated in the simulation, resulting in less electrical energy in the plasma arc and a longer discharge duration compared to the experiment.

Figure 12 shows comparisons between experiment and simulation for all the condition tested. The arc length and stretch distance from the simulations show dependence on both pressure and velocity. The simulation results show good agreement with the experiments especially in the early stage of the discharge until 1 ms before restrike/short-circuit occurs. Although the estimated arc stretch behavior at the later stage of discharge is different from actual arc stretch in the experiment, the early stage of discharge is of more interest in spark ignition systems for flame kernel formation. Also, electrical power from spark discharge, which is the product of voltage and current, is higher at the beginning of discharge as the current decreases monotonically during discharge.

Voltage also increases as the spark column stretches. However, the length or volume of the arc also increase for a stretched arc. Therefore, electrical power per unit length or volume does not change much with a stretched arc for the same current value. Electrical power per unit length or volume dominantly depends on the magnitude of the current. Therefore, we can conclude that the estimation or simulation of spark ignition at the early stage of discharge is more important in terms of voltage, current, and arc propagation. Our suggested arc propagation model does its job estimating arc stretch dependence on both pressure and velocity.

Another difference found between the experiment and the simulation is the arc length at 6 bar pressure. The simulation result underestimates arc length compared to the experiment for all three velocities. This may result from the fixed spark column diameter for all the pressures in the simulations. The actual spark column diameter changes with pressure and current. A larger spark column diameter at low pressure leads to a lower number density of electrons in equation (8), resulting in more stretch compared to a smaller spark column diameter.

Effect of the Electric Field

As the arc propagation model shown in equation (7) has two separate terms for flow and electric field, we can investigate the effect of the electric field by setting coefficient C_E to zero. Then the arc propagation is only determined by the crossflow. However, the flow term in the arc propagation model shown in equation (8) still has parameters determined from the current and voltage. The simulation was conducted for the same conditions as in the previous section.

Figure 13 shows results of simulations with and without the electric field term. The arc length and stretch distance are higher for simulations without the electric field than for simulations with the electric field. Arc propagation due to the electric field, shown in equation (8), acts against the arc propagation due to crossflow, shown in equation (7). When the spark column is stretched due to crossflow, the electric field pulls the stretched arc back toward its original position. This action is the reason why the arc velocity is slower than the flow velocity, as found in [13,14,15]. The difference between with and without the electric field term becomes smaller as pressure increases and as velocity increases. This means the electric field term has a larger effect at low pressure and low velocity. Arc propagation by the electric field term is relatively constant, independent of pressure and velocity. However, arc propagation by the flow term depends on both the pressure and velocity. This simulation without the electric field term is not representative of actual arc propagation as we cannot have a spark column free from an electric field. However, this simulation provides insight about how the electric field plays a role against the crossflow between the gap.

To see the effects of the time-step and mesh size on the simulation results, the time-step was varied between 0.05 to 0.5 μs and the mesh size was varied between 0.25 to 0.75 μm. The results are shown in Figures 14 and 15. A time-step of 0.05, 0.1, and 0.2 μs showed similar arc propagation behavior in terms of the length and timing of a short-circuit. For mesh size, there were similarities for two close mesh sizes. Mesh sizes of 0.250 and 0.375 μm showed similar results while 0.5

FIGURE 13 Effect of electric field for various pressures and crossflow velocities (a) arc length and (b) stretch distance. Red: with electric field; blue: without electric field

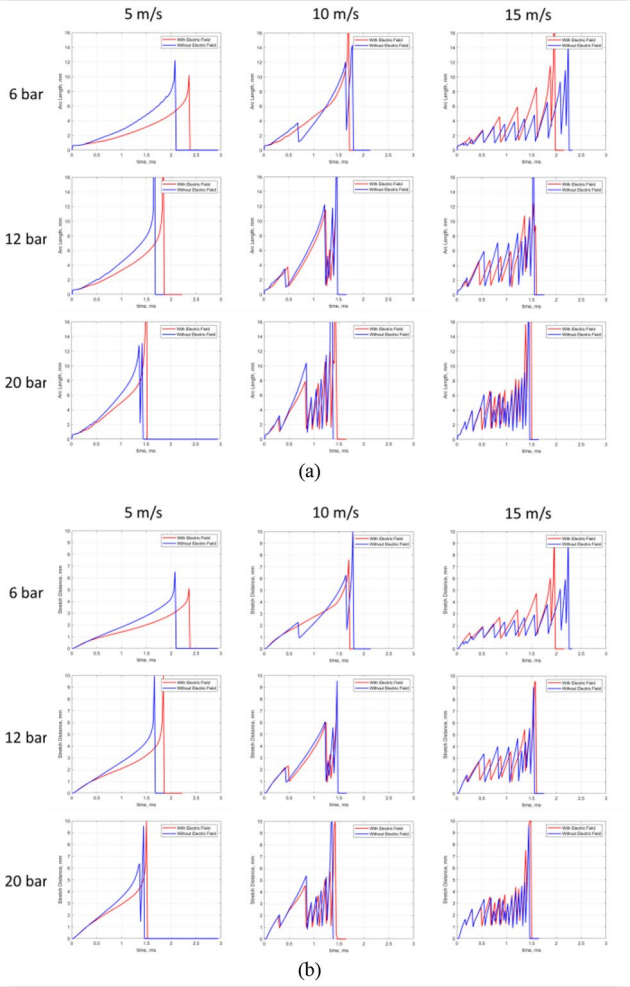

FIGURE 14 Simulation results with different time-step (a) arc length and (b) stretch distance

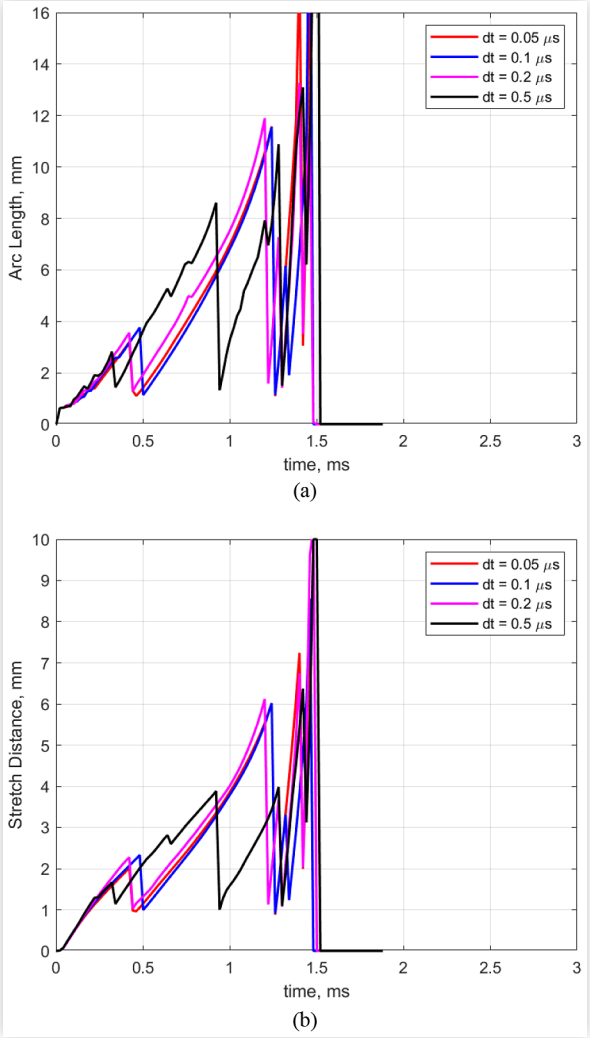

and 0.75 μm showed similarity in terms of length and timing of a short-circuit. It may seem that the simulation results with the presented model varies with time-step and mesh size. However, there are several constraints we can consider between the simulation and the actual arc propagation. The breakdown location was fixed at the center of the electrode surface in the simulation. In contrast, the actual breakdown location depends on the local electric field and surface conditions of the electrode, which we cannot simulate with CONVERGE CFD. This change in the breakdown location would also affect the local flow field between the gap and the arc propagation behavior. Considering these unpredictable characteristics of the breakdown event, selecting a proper range of the time-step and mesh size would still give reliable simulation results with the presented model.

Summary/Conclusions

Arc stretch and short-circuit behavior for pressures up to 20 bar and crossflow velocities up to 15 m/s was measured experimentally in a constant volume combustion vessel. Short-circuiting increased with decreasing pressure and increasing crossflow velocity. A special case for which the spark column maintained its stretched position was observed at 6 bar and 5 m/s. A new arc propagation model based on the mean-free-path of gas molecules and collisions between electrons and gas molecules was developed.

The new arc propagation model was based on the parameters we can obtain from the simulations of the flow field and the transient response of the ignition circuit. The new arc propagation model was integrated into the CONVERGE CFD software using a user defined function. Simulations were conducted for the same pressure and crossflow velocity conditions as the experiments. Simulation results were compared with experiments in terms of arc length and arc stretch distance. The simulation results showed good agreement with the experiments especially in the early stage of the discharge until 1 ms after breakdown.

Our new arc propagation model still needs improvement with respect to gap voltage of the stretched arc and spark column diameter. The underestimated gap voltage of the

FIGURE 15 Simulation results with different mesh size (a) arc length and (b) stretch distance

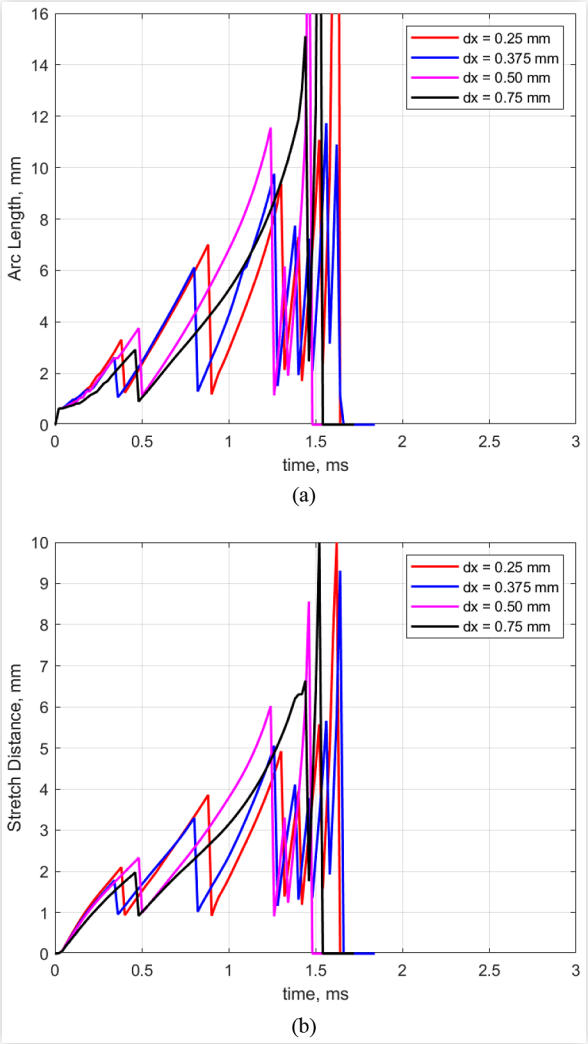

stretched arc in the present simulation resulted in longer discharge durations compared to the experiments. Additionally, a spark column diameter varying with pressure and current will also provide more accurate simulation results at low pressure.

The developed arc propagation model has two terms, arc stretch due to a flow term and arc stretch due to an electric field term. We could turn off the electric field term in the model by setting the coefficient to zero to examine the effect of the electric field on arc stretch. Eliminating the electric field in the simulation is not representative of the actual physics in spark ignition but it provides insight about how the electric field acts against the crossflow during arc propagation. The electric field pulls the stretched arc back toward its original location between the gap and this results in slower arc velocity than flow velocity, thereby explaining this phenomenon found by other researchers [13,14,15]. This electric field effect on arc propagation increases with decreasing flow velocity and decreasing pressure.

The simulation results with the developed arc propagation model showed good agreement with experiments for various pressures and velocities with the same single set of coefficients or parameters used in the model. The model does not require tuning or modification of coefficients for different pressures and crossflow velocities. This reveals that the suggested model can be applied to an entire engine simulation where both the pressure and crossflow velocity change during the simulation.

Arc propagation simulations from previous research studies, such as those mentioned in the Introduction, predict that the arc velocity is only related to the flow velocity. In those models, the arc moves at a velocity that is either the same as the flow velocity or empirically reduced to about half of the flow velocity. However, those concepts do not explain the arc propagation behavior under different pressures as we discovered from the experiments. The presented arc propagation model is based on collisions between the electrons and gas molecules which depends both on pressure and flow velocity. The presented arc propagation model is integrated into the CFD software, CONVERGE CFD to simulate the arc propagation under the presence of crossflow. Similar simulation could be done using the thermal plasma solver, VisSpark. However, the VizSpark simulation requires much more time and computing resources than the presented simulations using CONVERGE CFD. The simulations took about 4 hours on a 128 core supercomputer. Similar simulation using VizSpark required 4 days on a less powerful computer. A rough estimate for the VizSpark simulation time using the same 128 core supercomputer is about 30 hours.

The presented arc propagation model is part of a comprehensive ignition model that consists of an ignition circuit model, arc propagation model and energy deposition model. The ignition circuit model simulates the voltage and current in the ignition circuit and the plasma arc across the electrodes, and thus determines the amount of electrical energy delivered to the gap. The arc propagation model simulates the behavior of plasma arc between the electrodes, and thus determines the location of the energy deposition. The energy deposition model simulates the amount of thermal energy delivered to the gas from the electrical energy within the plasma arc. The energy deposition model is still under development for better prediction of the electrical-to-thermal energy conversion for a stretched arc. This comprehensive ignition model can be coupled to the existing combustion model within CONVERGE CFD to simulate combustion within a spark ignition engine.

References

1. Fan, L., Li, G., Han, Z., and Reitz, R., "Modeling Fuel Preparation and Stratified Combustion in a Gasoline Direct Injection Engine," SAE Technical Paper 1999-01-0175, 1999, https://doi.org/10.4271/1999-01-0175.
2. Duclos, J.M. and Colin, O., "Arc and Kernel Tracking Ignition Model for 3D Spark-Ignition Engine Calculations," *Int. Symp. Diagn. Model. Combust. Intern. Combust. Engines* 1 (2001): 46.
3. Dahms, R.N., Fansler, T.D., Drake, M.C., Kuo, T.-W. et al., "Modeling Ignition Phenomena in Spray-Guided Spark-Ignited Engines," *Proc. Combust. Inst.* 32 (2009): 2743-2750, doi:10.1016/j.proci.2008.05.052.

4. Lucchini, T., Cornolti, L., Montenegro, G., D'Errico, G. et al., "A Comprehensive Model to Predict the Initial Stage of Combustion in SI Engines," SAE Technical Paper 2013-01-1087, 2013, https://doi.org/10.4271/2013-01-1087.
5. Richards, K.J., Senecal, P.K., and Pomraning, E., *CONVERGE Users Guide & Reference Manual (Version 1.4.1)* (Middleton, WI: Convergent Science Inc., 2012)
6. Yang, X., Solomon, A., and Kuo, T., "Ignition and Combustion Simulations of Spray-Guided SIDI Engine Using Arrhenius Combustion with Spark-Energy Deposition Model," SAE Technical Paper 2012-01-0147, 2012, https://doi.org/10.4271/2012-01-0147.
7. Scarcelli, R., Zhang, A., Wallner, T., Som, S. et al., "Development of a Hybrid Lagrangian-Eulerian Model to Describe Spark-Ignition Processes at Engine-like Turbulent Flow Conditions," in: *ASME 2018 Internal Combustion Engine Division Fall Technical Conference*, (2018), doi:10.1115/ICEF2018-9690.
8. Sforza, L., Lucchini, T., Onorati, A., Zhu, X. et al., "Modeling Ignition and Premixed Combustion Including Flame Stretch Effects," SAE Technical Paper 2017-01-0553, 2017, https://doi.org/10.4271/2017-01-0553.
9. Masuda, R., Sayama, S., Fuyuto, T., Nagaoka, M. et al., "Application of Models of Short Circuits and Blow-Outs of Spark Channels under High-Velocity Flow Conditions to Spark Ignition Simulation," SAE Technical Paper 2018-01-1727, 2018, https://doi.org/10.4271/2018-01-1727.
10. Arai, R., Nabae, Y., Uekusa, R., Murakami, H. et al., "Numerical Modeling of Spark Path with Stretching and Short Circuit in Three-Dimensional Flow," SAE Technical Paper 2021-01-1164, 2021, https://doi.org/10.4271/2021-01-1164.
11. Kim, K., Tambasco, C., Hall, M.J., Matthews, R.D. et al., "Multi-Dimensional Spark Ignition Model with Distributed Energy Input and Integrated Circuit Model," SAE Technical Paper 2021-01-0405, 2021, https://doi.org/10.4271/2021-01-0405.
12. Mantel, T., "Three Dimensional Study of Flame Kernel Formation around a Spark Plug," SAE Technical Paper 920587, 1992, https://doi.org/10.4271/920587.
13. Kim, J. and Anderson, R., "Spark Anemometry of Bulk Gas Velocity at the Plug Gap of a Firing Engine," SAE Technical Paper 952459, 1995, https://doi.org/10.4271/952459.
14. Gardiner, D., Wang, G., Bardon, M., LaViolette, M. et al., "An Experimental Study of Spark Anemometry for in-Cylinder Velocity Measurements," *J. Eng. Gas Turbines Power* 130, no. 4 (2008): 042801, doi:10.1115/1.2898835.
15. Shiraishi, T., Teraji, A., and Moriyoshi, Y., "The Effects of Ignition Environment and Discharge Waveform Characteristics on Spark Channel Formation and Relationship between the Discharge Parameters and the EGR Combustion Limit," *SAE Int. J. Engines* 9, no. 1 (2016), doi:10.4271/2015-01-1895.
16. Sandhu, N., Yu, X., Yang, Z., Dev, S. et al., "An Investigation of Near-Spark-Plug Flow Field and its Effect on Spark Behavior," SAE Technical Paper 2019-01-0718, 2019, https://doi.org/10.4271/2019-01-0718.
17. Huang, S., Li, T., Wang, N., Wang, X. et al., "Experimental Study on the Characteristics of Short Circuits and Restrikes of Spark Channels," SAE Technical Paper 2020-01-1123, 2020, https://doi.org/10.4271/2020-01-1123.
18. Wörner, M. and Rottenkolber, G., "Voltage Rise Anemometry in Turbulent Flows Applied to Internal Combustion Engines," *Experiments in Fluids* 62 (2021): 132, doi:10.1007/s00348-021-03226-3.
19. Sayama, S., Kinoshita, M., Mandokoro, Y., Masuda, R. et al., "Quantitative Optical Analysis and Modelling of Short Circuits and Blow-Outs of Spark Channels under High-Velocity Flow Conditions," SAE Technical Paper 2018-01-1728, 2018, https://doi.org/10.4271/2018-01-1728.
20. Zembi, J., Battistoni, M., Mariani, F., Irimescu, A. et al., "Pressure and Flow Field Effects on Arc Channel Characteristics for a J-Type Spark Plug," SAE Technical Paper 2022-01-0436, 2022, https://doi.org/10.4271/2022-01-0436.
21. Colin, O. and Truffin, K., "A Spark Ignition Model for Large Eddy Simulation Based on an FSD Transport Equation (ISSIM-LES)," *Proceedings of the Combustion Institute* 33, no. 2 (2011): 3097-3104, doi:10.1016/j.proci.2010.07.023.
22. Tambasco, C., Li, D., Hall, M., and Matthews, R., "Spark Ignition Discharge Characteristics under Quiescent Conditions and with Convective Flows," SAE Technical Paper 2021-01-1157, 2021, https://doi.org/10.4271/2021-01-1157.
23. Kim, K., Hall, M.J., Wilson, P.S., and Matthews, R.D., "Arc-Phase Spark Plug Energy Deposition Characteristics Measured Using a Spark Plug Calorimeter Based on Differential Pressure Measurement," *Energies* 13 (2020): 3550, doi:10.3390/en13143550.

Contact Information

Prof. Matthew J. Hall
mjhall@mail.utexas.edu
The University of Texas at Austin
Department of Mechanical Engineering
204 E. Dean Keeton St. C2200
Austin, TX 78712

Acknowledgments

This project was made possible through funding provided by Cummins Inc. through the University of Texas at Austin's site of the NSF Center for Efficient Vehicles and Sustainable Transportation Systems (EVSTS). The authors wish to express their gratitude to Sachin Joshi, Daniel J. O'Connor and Douglas L. Sprunger of Cummins Inc. for many helpful discussions.

The Texas Advanced Computing Center (TACC) of the University of Texas at Austin provided the computational resources for the simulations. Those simulations would not have been possible without their continued support.

Definitions/Abbreviations

UDF - User Defined Function

CFD - Computational Fluid Dynamics

DPIK - Discrete Particle Ignition Kernel

AKTIM - Arc and Kernel Tracking Ignition Model

SparkCIMM - Spark Channel Ignition Monitoring Model

LESI - Lagrangian-Eulerian Spark-Ignition

DNS - Direct Numerical Simulation

HWA - Hot Wire Anemometry

PIV - Particle Image Velocimetry

ISSIM - Imposed Stretch Spark Ignition Model

FPS - Frames Per Second

TACC - Texas Advanced Computing Center

ISSN 0148-7191